Interactions between the secreted protein Amalgam, its transmembrane receptor Neurotactin and the Abelson tyrosine kinase affect axon pathfinding

Eric C. Liebl[1,‡], R. Grant Rowe[1], David J. Forsthoefel[2], Amanda L. Stammler[1], Erica R. Schmidt[1,*], Michelle Turski[2,†] and Mark A. Seeger[2]

[1]Department of Biology, Denison University, Granville, OH 43023, USA
[2]Department of Molecular Genetics and The Center for Molecular Neurobiology, The Ohio State University, Columbus, OH 43210, USA
*Present address: College of Medicine, The Ohio State University, Columbus, OH 43210, USA
†Present address: University Program in Genetics, Duke University, Durham, NC 27708, USA
‡Author for correspondence (e-mail: liebl@denison.edu)

SUMMARY

Two novel dosage-sensitive modifiers of the Abelson tyrosine kinase (*Abl*) mutant phenotype have been identified. Amalgam (Ama) is a secreted protein that interacts with the transmembrane protein Neurotactin (Nrt) to promote cell:cell adhesion. We have identified an unusual missense *ama* allele, *ama^M109^*, which dominantly enhances the *Abl* mutant phenotype, affecting axon pathfinding. Heterozygous null alleles of *ama* do not show this dominant enhancement, but animals homozygous mutant for both *ama* and *Abl* show abnormal axon outgrowth. Cell culture experiments demonstrate the Ama^M109^ mutant protein binds to Nrt, but is defective in mediating Ama/Nrt cell adhesion. Heterozygous null alleles of *nrt* dominantly enhance the *Abl* mutant phenotype, also affecting axon pathfinding. Furthermore, we have found that all five mutations originally attributed to *disabled* are in fact alleles of *nrt*. These results suggest Ama/Nrt-mediated adhesion may be part of signaling networks involving the Abl tyrosine kinase in the growth cone.

Key words: Neural development, Axon pathfinding, Abelson tyrosine kinase, *Abl*, *amalgam*, *disabled*, *neurotactin*, *Drosophila melanogaster*

INTRODUCTION

The cytoplasmic tyrosine kinase Abl is incorporated into multiple signaling networks, including those regulating cell cycle progression, cytoskeletal dynamics and axon outgrowth (Van Etten, 1999). In *Drosophila*, the Abl kinase is localized to the axons of the central nervous system (CNS) during embryogenesis (Bennett and Hoffmann, 1992; Gertler et al., 1989). Thus, genetic screens for second site mutations that alter the *Abl* mutant phenotype in *Drosophila* have been instrumental in identifying many components of the networks regulating axon extension (Hoffmann, 1991; Lanier and Gertler, 2000). In these genetic screens, a variety of different experimental approaches have been taken; both enhancers and suppressors of the *Abl* mutant phenotype have been identified, and genes that show dosage-sensitive interactions with *Abl*, as well as genes that alter the *Abl* mutant phenotype only when homozygous mutant, have been uncovered.

One theme that has emerged from these genetic analyses is that the Abl kinase may influence axon outgrowth by affecting cytoskeletal dynamics. Dosage-sensitive genetic interactions affecting axon outgrowth have been found between *Abl* and *enabled* (*ena*), with *ena* being a dominant suppressor of the *Abl* mutant phenotype (Gertler et al., 1990). *ena* encodes an Abl substrate with multiple SH3-binding sites (Gertler et al., 1995) and was the first identified member of the Ena/VASP family (Lanier and Gertler, 2000). Its mammalian homolog Mena plays roles in axon guidance and cell migration by affecting actin filament assembly (Bear et al., 2000; Bear et al., 2002; Gertler et al., 1996; Goh et al., 2002; Lanier et al., 1999; Renfranz and Beckerle, 2002). Dosage-sensitive genetic interactions affecting axon outgrowth have also been found between *Abl* and *trio*, with *trio* being a dominant enhancer of the *Abl* mutant phenotype (Liebl et al., 2000). *trio* encodes a protein with multiple domains, including an SH3 domain and two guanine-nucleotide-exchange-factor domains (Awasaki et al., 2000; Bateman et al., 2000; Liebl et al., 2000; Newsome et al., 2000), which can function to reorganize the actin cytoskeleton (Newsome et al., 2000). *Abl* and the profilin homolog *chickadee* show dosage-sensitive genetic interactions affecting axon outgrowth, with *chickadee* dominantly enhancing a motoneuron phenotype in *Abl* mutants (Cooley et al., 1992; Wills et al., 1999). A protein with similarities to neurofilaments, *failed axon connections* (*fax*), has also been identified as a dominant enhancer of the *Abl* mutant phenotype (Hill et al., 1995).

Abl has recently been shown to have multiple interactions with *robo* signaling networks. *robo* encodes the transmembrane receptor for Slit and is involved in regulating

axon midline crossing (Kidd et al., 1999; Seeger et al., 1993). Bashaw et al. found that in a background sensitized by overexpression of Abl, *robo* serves as a dominant enhancer with heterozygous mutations strongly increasing inappropriate midline crossing in the CNS, leading to a model whereby Robo is negatively regulated by Abl phosphorylation (Bashaw et al., 2000). Others have also shown that Abl and Capt (a protein involved in actin cytoskeleton dynamics) may be involved in restricting midline crossing in response to Slit (Willis et al., 2002). Additionally, it has been shown that Abl may phosphorylate β-catenin, negatively regulating N-cadherin function in response to Slit-activated Robo (Rhee et al., 2002).

A dosage-sensitive genetic interaction that affects axon outgrowth between *Abl* and *disabled* (*dab*) has been reported, with *dab* dominantly enhancing the *Abl* mutant phenotype (Gertler et al., 1989). *dab*, which is the ortholog of murine *Dab1* (Howell et al., 1997) or *scrambler* (Ware et al., 1997), encodes a tyrosine phosphorylated adaptor protein containing a phosphotyrosine-binding (PTB) domain (Gertler et al., 1993; Howell et al., 1997). Work in the murine system has shown Dab1 plays a role in neuronal migration (Gallagher et al., 1998; Ware et al., 1997).

This report now expands and modifies the cast of characters included in axon extension networks involving Abl. We show that *amalgam* (*ama*) and *neurotactin* (*nrt*) interact genetically with *Abl*. *ama* encodes a secreted protein with three Ig-domains (Fremion et al., 2000; Seeger et al., 1988), while *nrt* encodes a transmembrane protein with a catalytically inactive cholinesterase domain (Barthalay et al., 1990; de la Escalera et al., 1990; Hortsch et al., 1990) recently identified as the in vivo receptor for Amalgam (Fremion et al., 2000). We have identified an unusual missense allele of *ama* generated in genetic screens for strong dominant enhancers of the *Abl* mutant phenotype. In addition, our molecular characterization of chromosomes carrying dominant enhancers of the *Abl* mutant phenotype, originally identified as *dab* alleles, has shown that these chromosomes in fact are mutant for *nrt*. These mutations all show dosage-sensitive effects on axon pathfinding in the *Abl* mutant background. As the binding of Amalgam to Neurotactin promotes cell adhesion (Fremion et al., 2000), these genetic interactions define an additional role for the Abl tyrosine kinase in axon guidance.

MATERIALS AND METHODS

Genetics

All genetic crosses were carried out using standard cornmeal-yeast medium in humidified, 25°C incubators. The *ama^M109* allele was recovered in genetic screens which mutagenized the *Abl^1* chromosome with ethylmethane sulfonate (EMS) as previously described (Gertler et al., 1989; Hill et al., 1995). For all dosage-sensitive genetic tests, stocks were balanced over the *TM6, B, Hu, e, Tb, ca* balancer chromosome. The percent of expected Tb^+ pupae recovered from each cross was calculated by dividing the total number of Tb^+ pupae by one half the total number of Tb pupae. The percent of expected Hu^+ adults recovered from each cross was calculated in the same way. All data reported represent a minimum of 400 progeny counted from each cross.

Sequence analysis

In all cases genomic DNA was isolated from pupae or animals hemizygous for the gene of interest. All amplifications for sequence analysis were carried out using polymerase with proofreading activity (Advantage HF2, BD BioSciences/Clontech, Palo Alto, CA). The *ama* ORF was amplified as one 1.3 kb piece. The *nrt* ORF was amplified as four overlapping fragments, each ~800 bp. The *dab* ORF was amplified as eleven fragments, each ~850 bp. Not all of these fragments overlapped, as not all of the two large introns (intron 1 and intron 4) of *dab* were sequenced. Sequences of primers used are available on request. All fragments showing a deviation from wild type were independently re-amplified and re-sequenced.

RNAi and immunostaining

dsRNA was generated and injected into embryos as described (Kennerdell and Carthew, 1998), with the exception that embryos were injected dorsally. Primer sequences used to generate templates for in vitro transcription of *Abl*, *nrt* and *ama* are available upon request. After injection, embryos were raised at 18°C, and harvested at stage 14-15 for mAb BP102 immunohistochemistry (Patel et al., 1987). mAbs BP102 and BP106 were obtained from the Developmental Studies Hybridoma Bank (University of Iowa, Iowa City, IA). Anti-β-galactosidase mAb (Promega, Madison WI) was used to detect *lacZ* expression from enhancer-trap-containing balancer chromosomes to distinguish the genotypes of the embryos.

S2 cell assays

All *ama* and *nrt* alleles were cloned into the pMET vector (Bunch et al., 1988), under the control of the metallothionine promoter. Stable S2 cell populations were derived by co-transfecting with pPC4 (Elkins et al., 1990) and selecting for α-amanitin resistance. Fragments containing the mutations associated with *ama^M109*, *nrt^M100* and *nrt^M221* were introduced into pMET-Ama, pMET-Ama-TM (Fremion et al., 2000) and pMET-Nrt constructs using available restriction enzyme sites and confirmed by DNA sequencing. For aggregation assays, conditioned media was generated by inducing expression of pMET-Ama, pMET-Ama^M109 or naïve S2 cells with 0.7 mM CuSO4 overnight. Ama-expressing cells were then removed by centrifugation. The conditioned media was added to naïve S2 cells or cells transfected with different pMET-Nrt constructs. The addition of conditioned media containing 0.7 mM CuSO4 initiated expression of pMET-Nrt. Aggregation assays were conducted in six-well microtiter plates on a rotary shaker at 80 rpm with ~5×10^6 cells per ml. Particles (cells and aggregates) were counted on a hemacytometer at t=0, 4 and 8 hours. Cells transfected with pMET-Ama-TM and pMET-Ama^M109-TM were induced directly with 0.7 mM CuSO4 at the beginning of the aggregation assay. Accumulation of these membrane-anchored forms of Ama was detected with mAb BP104, which recognizes an epitope in the cytoplasmic domain of Nrg (Hortsch et al., 1995).

For cell pull-down assays, expression of Nrt was induced with overnight exposure to 0.7 mM CuSO4. Nrt-expressing cells (5×10^6 per ml) were recovered by low-speed centrifugation and resuspended in Ama-conditioned media (see above). Cells were allowed to aggregate for 60 minutes and then recovered by centrifugation. Cell pellets were washed once with Schneiders media, re-pelleted and re-suspended in Laemmli lysis buffer. Equivalent numbers of cells were used in all assays. Equal volumes of cell lysates were loaded for immunoblot analysis. Nrt was detected with mAb BP106 (Hortsch et al., 1990). Ama was detected with rabbit anti-Ama antisera (Seeger et al., 1988).

RESULTS

An allele of *amalgam* was isolated as a novel dominant enhancer of the *Abl* mutant phenotype

Similar to the genetic screens that yielded alleles of *fax* and *trio*, third chromosomes carrying the *Abl^1* allele were mutagenized with EMS, and dominant mutations that shifted
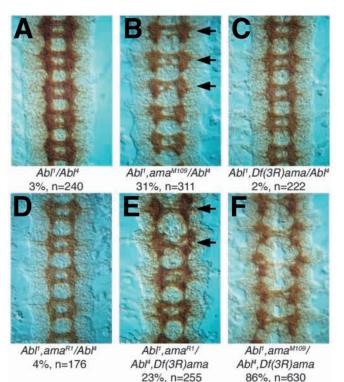
Table 1. Dosage-sensitive modification of the *Abl* mutant phenotype by *ama* mutations

Genotype	Dose of *Abl*	Dose of *ama*	Pupae*	Adults*
Abl¹/Abl⁴	0	2	96	56
Abl¹, ama^{M109}/Abl⁴	0	1	0	0
P[Abl⁺]; Abl¹, ama^{M109}/Abl⁴	1	1	103	116
Abl¹, Df(3R)ama/Abl⁴	0	1	92	22
Abl¹, ama^{R1}/Abl⁴	0	1	104	67

*The percent of the expected progeny class of both pupae and viable adults of the indicated genotype is shown. A minimum of 400 animals was counted in each cross.

Fig. 1. CNS phenotypes of *Abl* and *ama* mutants. Embryos from stage 14/15 were stained with mAb BP102 and CNSs were dissected. Representative examples of the overall phenotype associated with each genotype are shown. (A) *Abl¹/Abl⁴*, (B) *Abl¹, ama^{M109}/Abl⁴*, (C) *Abl¹, Df(3R)ama/Abl⁴*, (D) *Abl¹, ama^{R1}/Abl⁴*, (E) *Abl¹, ama^{R1}/Abl⁴, Df(3R)ama*, (F) *Abl¹, ama^{M109}/Abl⁴, Df(3R)ama*. Percentages below each panel indicate the percent of segments with commissure defects; *n*=total segments scored. Arrows in B,E show typical examples of segments scored as having defective commissures.
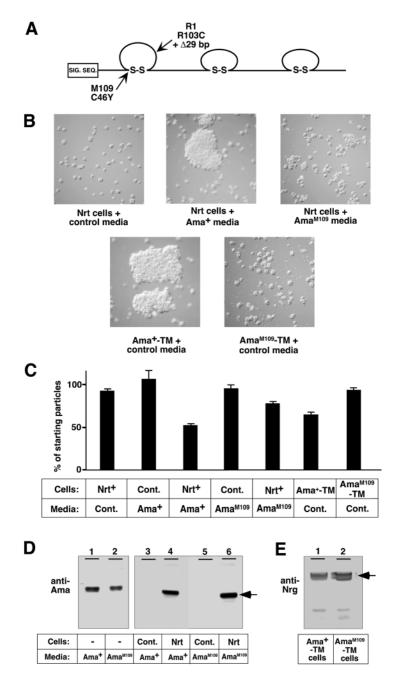
the lethality associated with the *Abl* mutant phenotype to pre-pupal stages were recovered (Gertler et al., 1989; Hill et al., 1995). A mutation, originally designated as *M109*, was isolated. Meiotic mapping of *M109* placed this mutation between *st* and *th*, at ~47cM. Complementation analysis across this region showed that *M109* failed to complement *Df(3R)MAP11*, a well characterized deficiency that removes *zen*, *bcd*, *ama* and *Dfd* (Diederich et al., 1989). *Abl¹*, *M109/Df(3R)MAP11* embryos developed normal cuticles (data not shown), making it unlikely that *M109* was an allele of *zen* or *Dfd*. Based upon the genetic interaction between *Abl* and *M109*, and the similar spatial and temporal expression patterns of *Abl* and *ama* (Bennett and Hoffmann, 1992; Seeger et al., 1988), we hypothesized that *M109* may be an *ama* allele. We tested this directly by amplifying the *ama* open reading frame (ORF) from *Abl¹*, *M109/Df(3R)MAP11* 'escaper' animals, and comparing it to the *ama* ORF amplified from the parental *Abl¹* chromosome. A single alteration was detected from the *Abl¹*, *M109* chromosome; residue 46 was changed from cysteine to tyrosine (Fig. 2A). As a disulfide bond between C46 and C117 is believed to stabilize the first Ig domain of Ama (Seeger et al., 1988), the C46Y change probably results in a dramatically altered protein product. Having colocalized a missense mutation within a critical residue in the *ama* ORF with the *M109* mutation, we now refer to this mutant allele as *ama^{M109}*.

ama^{M109} was found to be a strong dominant enhancer of the *Abl* mutant phenotype. Unlike alleles of *fax* or *trio* that reduce the number of *Abl* mutant animals that survive to pupation (Hill et al., 1995; Liebl et al., 2000), *ama^{M109}* completely eliminated this class of pupae (Table 1). However, similar to alleles of *fax* and *trio*, the dominant enhancement by *ama^{M109}* of the *Abl* mutant phenotype was rescued by one wild-type allele of *Abl* (Table 1), showing the haploinsufficiency of *ama^{M109}* to be dependent on *Abl* mutations. Consistent with the *ama^{M109}* mutation identifying a gene product involved in axon guidance, the shift of the *Abl* mutant lethal phase corresponded to an increase in axon outgrowth defects. This was most easily quantified by staining embryos with mAb BP102 in order to visualize the axon scaffold, and counting segments with defective commissures. Segments with missing, fused or other obvious commissural pathfinding errors were scored as defective, as illustrated in Figs 1 and 3. In *Abl* mutant embryos (*Abl¹/Abl⁴*) only 3% of the segments had defective commissures (*n*=240), and the CNS had an essentially wild-type appearance (Fig. 1A). However, in *ama^{M109}/ama⁺*, *Abl* mutant embryos (*Abl¹*, *ama^{M109}/Abl⁴*), 31% of segments had commissure defects (*n*=311; Fig. 1B).

A null allele of *ama* did not enhance the *Abl* mutant phenotype

To date, the only *ama* allele recovered as a dominant enhancer of the *Abl* mutant phenotype is *ama^{M109}*. To test whether a null allele of *ama* could function as a dominant enhancer of the *Abl* mutant phenotype, we generated a recombinant *Abl¹*, *Df(3R)ama* chromosome. *Df(3R)ama* is a small deletion that removes *zen*, *bcd* and *ama* (Fremion et al., 2000). Neither survival to pupation, nor the percentage of segments with commissure defects was dramatically altered between *Abl* mutant animals and *Abl* mutant animals heterozygous null for *ama*. Animals of the genotype *Abl¹/Abl⁴* gave 96% of the expected pupae (Table 1), and 3% of the segments in such embryos showed commissure defects (*n*=240; Fig. 1A). Animals of the genotype *Abl¹*, *Df(3R)ama/Abl⁴* produced 92% of the expected pupae (Table 1), and 2% of the segments in such embryos showed commissure defects (*n*=222; Fig. 1C). We therefore concluded that a null allele of *ama* was not a dominant enhancer of the *Abl* mutant phenotype.

Null point-alleles of *ama* have never been described. In order to generate such alleles, we capitalized on our observation that a null allele of *ama* was not a dominant enhancer of the *Abl* mutant phenotype, and re-mutagenized the *Abl¹*, *ama^{M109}* chromosome with EMS, screening for revertants of the

dominant enhancement by ama^{M109} of the *Abl* mutant phenotype. Ten EMS-induced intragenic revertants of ama^{M109}, all carrying the C46Y *M109* mutation in addition to new alterations, have been recovered in this screen. Interestingly, nine of these revertants carry single missense mutations. We are currently characterizing the proteins encoded by these altered *ama* genes. However, one allele of *ama*, an R103C missense allele combined with a 29 bp deletion beginning in the P114 codon, was also generated. This is a null allele, as it can code for only the first 113 residues of Ama (with C46Y and R103C) followed by 54 novel residues due to the frameshift of the 29 bp deletion. We have named this revertant allele ama^{R1} (Fig. 2A).

We have found that 4% of the segments of embryos of the genotype Abl^1, ama^{R1}/Abl^4 have defective commissures

(n=176; Fig. 1D), and all of these embryos survive to pupation (Table 1). In both cases, these data were very similar to the characteristics of the Abl^1, $Df(3R)ama$ chromosome (2% defective segments, 92% survival to pupation) and very different from the parental Abl^1, ama^{M109} chromosome (31% defective segments, 0% survival to pupation). We have observed better survival to adulthood of Abl^1, ama^{R1}/Abl^4 animals as compared to Abl^1, $Df(3R)ama/Abl^4$ animals (Table 1), but as the Abl^1, $Df(3R)ama$ chromosome was generated by recombination and the $Df(3R)ama$ deficiency is a multigenic deletion, this discrepancy may be attributable to differences in genetic backgrounds, and we have not investigated this observation further. The recovery of a null allele of *ama* in a screen for revertants of the dominant enhancement by ama^{M109} of the *Abl* mutant phenotype confirms our identification of the ama^{M109} allele as the causative mutation responsible for the dominant enhancement of the *Abl* mutant phenotype.

Biochemical and genetic characterization of the ama^{M109} allele

Fremion et al. (Fremion et al., 2000) have demonstrated that Ama binding to Nrt mediates cell:cell adhesion. These authors have also shown that Ama proteins can self-associate, suggesting a model whereby the binding of Ama to cell-surface Nrt, as well as Ama:Ama homophilic binding somehow cooperate to promote cell:cell adhesion. Similar to Fremion et al., we have employed two assays to examine the biochemical behavior of Ama proteins. First, using S2 cells engineered to express wild-type Nrt (see Materials and Methods), we have tested whether media

Fig. 2. Biochemical characterization of Ama+ and Ama^{M109}.
(A) The organization of Ama with its signal sequence and three Ig domains (loops). The N terminus is towards the left. The ama^{M109} and the ama^{R1} mutations are also indicated.
(B) Representative photomicrographs showing our S2 cell adhesion assay at t=8 hours. In the top three panels, all cells were engineered to express wild-type Nrt and were exposed to either control (left), Ama+-containing (center) or Ama^{M109}-containing (right) conditioned media. In the bottom two panels, cells were engineered to express membrane-anchored forms of Ama.
(C) Quantification of our S2 cell adhesion assays. Bars represent the percent of total particles at t=0 hours counted at t=8 hours. Values represent the average of two independent experiments; error bars show the standard error of the mean. (D) Anti-Ama immunoblots. The arrow indicates the mobility of full-length Ama. Lanes 1, 2: equal amounts of Ama+-conditioned media or of Ama^{M109}-conditioned media were resolved. These lanes show that comparable amounts of Ama were present in both types of conditioned media. Lanes 3-6: immunoblots of S2 cell lysates from cell pull-down assays. Equivalent amounts of cell lysates were loaded in each lane. Lane 3: naïve S2 cells exposed to Ama+-conditioned media. Lane 4: Nrt-expressing S2 cells exposed to Ama+-conditioned media. Lane 5: naïve S2 cells exposed to Ama^{M109}-conditioned media. Lane 6: Nrt-expressing S2 cells exposed to Ama^{M109}-conditioned media. These lanes show that Ama+ and Ama^{M109} bound specifically to S2 cells expressing Nrt. (E) Anti-Nrg immunoblots. Equivalent amounts of cell lysates were loaded in each lane. The arrow indicates the mobility of the Ama-Nrg fusion protein. Lane 1: S2 cells expressing Ama+-TM. Lane 2: S2 cells expressing Ama^{M109}-TM. These lanes show equivalent amounts of these chimeric proteins were expressed.

containing secreted Ama can mediate cell:cell adhesion. Cell adhesion was quantified in these assays by counting total particles over time, with particles defined as single cells and cell aggregates regardless of size. A reduction in particle number indicated cell:cell adhesion, as free cells aggregated into clusters. As part of this assay, we also indirectly monitored Ama:Nrt binding by isolating cells exposed to Ama-containing media, and testing for the specific binding of Ama to Nrt-expressing cells in a cell pull-down assay. For our second assay, we generated Ama proteins fused to the transmembrane and cytoplasmic domains of Neuroglian, thus creating a membrane-anchored Ama (Fremion et al., 2000). By inducing the expression of these chimeric proteins, we tested whether Ama:Ama interaction occurred by monitoring cell aggregation. Both Ama$^+$ and Ama^{M109} were tested in these assays.

While naïve S2 cells did not express Ama, after transfection with the appropriate expression plasmid both Ama$^+$ and Ama^{M109} were produced as stable, secreted proteins at comparable levels (Fig. 2D, lanes 1, 2). Naïve S2 cells did not express Nrt (Fig. 4C, lane 1). Therefore, neither Nrt-expressing S2 cells exposed to naïve supernatant, nor naïve S2 cells exposed to Ama$^+$ or Ama^{M109}-containing supernatant showed aggregation (Fig. 2C), and naïve S2 cells did not bind Ama (Fig. 2D, lanes 3, 5). Ama$^+$ did bind to Nrt-expressing S2 cells (Fig. 2D, lane 4), and supported their aggregation, with large aggregates of cells forming (Fig. 2B); total particle number was reduced by 48% over the 8 hour assay (Fig. 2C). Ama^{M109} also bound Nrt-expressing S2 cells (Fig. 2D, lane 6), but the aggregation it induced was clearly different from that seen with Ama$^+$ with the aggregates that formed being small (Fig. 2B). In this case, total particle number was reduced by only 23% over the 8 hour assay (Fig. 2C). In addition, Ama^{M109}-induced aggregates were less stable, disappearing after 24 hours, while Ama$^+$-induced aggregates persisted beyond 24 hours (data not shown).

Fig. 2 also shows our tests of the ability of Ama$^+$ and Ama^{M109} to self-aggregate when expressed as transmembrane chimeras. Both were expressed at comparable levels (Fig. 2E, lanes 1, 2). Consistent with its ability to support Nrt-mediated cell adhesion as a secreted protein, Ama$^+$-TM demonstrated homophilic association (Fig. 2B), with total particle number reduced by 34% over the 8 hour assay (Fig. 2C). However, Ama^{M109}-TM did not induce cell aggregation in this assay (Fig. 2B,C). Taken together, these results suggest that the first Ig-domain of Ama, which is stabilized by the disulfide bond between C46 and C117, is crucial for Ama:Ama interaction, but not for Ama:Nrt interaction. These results also support a model in which Ama:Ama interaction is important for normal Ama:Nrt-mediated cell adhesion (Fremion et al., 2000).

Given the ability of Ama^{M109} to bind Nrt but mediate only limited cell:cell adhesion, and our observations that the ama^{M109} allele behaved as a dominant enhancer of the *Abl* mutant phenotype, while null alleles of *ama* did not, we wished to explore the genetic properties of the ama^{M109} mutation. The dominant activity of Ama^{M109} could be the result of dominant-negative effects. In this model, Ama^{M109} binding to Nrt exerts its influence by the exclusion of Ama$^+$ binding, precluding normal Ama$^+$-mediated cell:cell adhesion. Alternatively, the Ama^{M109} protein could have a more complex biochemical activity, actively producing phenotypic effects by occupying Nrt receptors. Using our ama^{R1} allele, we hypothesized that if

ama^{M109} behaved strictly as a dominant-negative, the ama^{R1}/Df(3R)ama and the ama^{M109}/Df(3R)ama phenotypes would be similar. We found, however, a dramatic difference between the ama^{R1}/Df(3R)ama and the ama^{M109}/Df(3R)ama phenotypes in an *Abl* mutant background. Animals of the genotype Abl^1, ama^{R1}/Abl^4, Df(3R)ama were found to have 23% of segments with defective commissures (n=255; Fig. 1E), while animals of the genotype Abl^1, ama^{M109}/Abl^4, Df(3R)ama had 86% of segments with defective commissures (n=630; Fig. 1F). We therefore concluded that Ama^{M109} exerts phenotypic effects even in the absence of Ama$^+$.

Elimination of Nrt strongly enhances the *Abl* mutant phenotype

Ama is a secreted protein, while Abl is a cytoplasmic tyrosine kinase. The transmembrane protein Nrt has been shown to be an in vivo receptor for Ama (Fremion et al., 2000). Given the strong genetic interaction between ama^{M109} and *Abl*, and the unusual genetic character of ama^{M109}, we were curious to test for genetic interactions between *nrt* and *Abl*. Although mutant alleles of *nrt* exist (Speicher et al., 1998), *nrt* lies just proximal to *Abl* on chromosome three, precluding the simple generation of an *Abl*-mutant, *nrt*-mutant chromosome by recombination. We therefore elected to use RNAi to generate Abl-null, Nrt-null embryos.
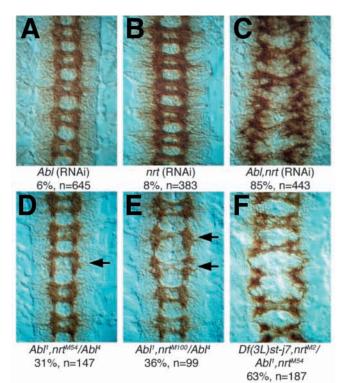
Embryos were injected with double-stranded RNA, fixed and mAb BP102 was used to visualize axon tracts in the CNS. As shown in Table 2 and Fig. 3, elimination of Abl, Ama or Nrt singly did not have a strong effect on the number of segments with commissure defects. Although in buffer-injected control embryos, 3% of their segments displayed commissure defects (n=833; Table 2), Abl-null embryos generated with RNAi showed commissure defects in 6% of their segments (n=645; Table 2; Fig. 3A). Ama-null embryos were found to have 3% of their segments with commissure defects (n=159; Table 2). In accordance with previous data (Speicher et al., 1998), Nrt-null embryos had mild CNS defects, with 8% of their segments having commissure defects (n=383; Table 2; Fig. 3B). Eliminating Abl and Ama together had a synergistic effect, with 32% of segments showing commissure defects (n=350; Table 2). Eliminating Abl and Nrt together had an even more dramatic effect, with 85% of segments showing commissure defects (n=443; Table 2; Fig. 3C). There was also a qualitative difference in the defects found, with the disruptions of the axon scaffold resulting from the elimination of Abl and Nrt being much more severe than with any other combination. Only in this background were breaks in

Table 2. Phenotypic effects of RNAi for *Abl*, *ama* and *nrt*

Double-stranded RNA injected	% defects*	n†
Buffer control	3	833
Abl	6	645
ama	3	159
nrt	8	383
Abl + ama	32	350
Abl + nrt	85	443

*The percent of the total segments that were judged to have defective commissures is shown. Commissures were defined as defective if more than 75% of commissural axons were absent, or clear pathfinding errors were present.

†Total number of segments scored.

Fig. 3. CNS phenotypes of *Abl* and *nrt* mutants. Mutants were either generated by RNAi (A-C) or by zygotic genotypes (D-F). Embryos from stage 14/15 were stained with mAb BP102, and CNSs were dissected. Representative examples of the overall phenotype associated with each genotype are shown. (A) *Abl* null, (B) *nrt* null, (C) *Abl* and *nrt* null, (D) *Abl¹, nrt^{M54}/Abl⁴*, (E) *Abl¹, nrt^{M100}/Abl⁴*, (F) *Df(3L)st-j7, nrt^{M2}/Abl¹, nrt^{M54}*. Percentages below each panel indicate the percent of segments with commissure defects; *n*=total segments scored. Arrows in D,E show typical examples of segments scored as having defective commissures.

longitudinal axon tracts between anterior and posterior commissures observed. In addition, many more disrupted segments were totally commissureless (Fig. 3C).

Identification of *nrt* as a dominant enhancer of the *Abl* mutant phenotype

As our RNAi experiments had shown a clear and strong synergistic effect on axon pathfinding when both Abl and Nrt were eliminated, we hypothesized that *nrt* may function as a dominant enhancer of the *Abl* mutant phenotype, similar to *fax*, *trio* and *ama^{M109}*. To test this hypothesis, we needed to generate an *Abl*-mutant, *nrt*-mutant chromosome. To achieve this, we initiated a genetic screen similar to that detailed by Speicher et al. (Speicher et al., 1998) in which the *Abl¹* chromosome was mutagenized with EMS so that chromosomes that no longer produced Nrt, as judged by reactivity with the anti-Nrt mAb BP106 (Hortsch et al., 1990), would be identified. We also noted, however, that *nrt* lies only ~55kb proximal to *dab* in polytene band 73C. To test the idea that perhaps some mutations originally attributed to *dab* could, in fact, be *nrt* alleles, we also screened all existing *dab* mutant chromosomes [*Df(3L)st-j7, dab^{M2}; Df(3L)st-j7, dab^{M29}; Abl¹, dab^{M54}; Abl¹, dab^{M100}; Abl¹, dab^{M221}*] for their ability to produce Nrt, as judged by mAb BP106 reactivity in embryos. Before

undertaking this analysis, we confirmed previous reports (Gertler et al., 1989) that these chromosomes showed dominant enhancement of the *Abl* mutant phenotype, and that this dominant effect was dependent on *Abl* mutations (Table 3). In addition, we confirmed previous reports (Gertler et al., 1989) that this enhancement of the *Abl* mutant phenotype was accompanied by axon pathfinding defects in the CNS (Fig. 3D,E).

Staining with mAb BP106 showed that embryos homozygous for *Df(3L)st-j7, dab^{M2}*, *Df(3L)st-j7, dab^{M29}* or the *Abl¹, dab^{M54}* chromosome failed to produce Nrt, identical to *In(3L)std11* control chromosomes. *In(3L)std11* removes *Abl*, *dab* and *nrt* (Belote et al., 1990; de la Escalera et al., 1990). By contrast, the *Abl¹, dab^{M100}*, the *Abl¹, dab^{M221}*, and the *Abl¹* and *Df(3L)st-j7* parental chromosomes produced Nrt (data not shown). As these preliminary results suggested that some chromosomes carrying dominant enhancers of the *Abl* mutant phenotype were Nrt-protein nulls, we abandoned our genetic screen and carried out careful molecular analyses of these chromosomes.

To explore the possibility further that some mutations attributed to *dab* could in fact be *nrt* alleles, we generated animals hemizygous for the *dab* and *nrt* alleles carried on these mutagenized chromosomes and sequenced both of these genes. For all five *dab* mutant chromosomes we recovered 'escaper' animals over *In(3L)std11* by supplying a single wild-type *Abl* transposon on the second chromosome. From the genomic DNA of these animals, we amplified and sequenced all exons and intron/exon boundaries of both *dab* and *nrt*.

For our sequence analysis of *dab*, we took the conceptual translation of the *dab* allele found under the Accession Number NM079395 (GenBank) as our wild-type benchmark. This would result in a Dab protein of 2224 residues. We found numerous polymorphisms in the *dab* alleles we sequenced compared with this wild-type benchmark. Some of these polymorphisms were common to all five alleles (N620T, V1061M, Y1241D, L1294Q, V1594A, D2089E). Some were specific to the individual parental chromosomes [*Abl¹*: A1978V, A2175V; *Df(3L)st-j7*: S203A, Q543L, A557T, Q993K]. However, in no case did we find a unique mutation that would suggest a mutant *dab* allele had been generated on any of these chromosomes carrying dominant enhancers of the *Abl* mutant phenotype.

For our sequence analysis of *nrt*, we took the conceptual translation of the *nrt* allele reported by Hortsch et al. (Hortsch et al., 1990) as our wild-type benchmark (GenBank Accession

Table 3. Dosage-sensitive modification of the *Abl* mutant phenotype by *nrt* mutations*

Genotype	Dose of *Abl*	Dose of *nrt*	Pupae[†]	Adults[†]
Abl¹/Abl⁴	0	2	72	57
Df(3L)st-j7/Abl⁴	0	2	110	66
Abl¹, nrt^{M54}/Abl⁴	0	1	0	0
P[Abl⁺]; Abl¹, nrt^{M54}/Abl⁴	1	1	92	88
Abl¹, nrt^{M100}/Abl⁴	0	1	0	0
Df(3L)st-j7, nrt^{M2}/Abl⁴	0	1	15	9
Df(3L)st-j7, nrt^{M29}/Abl⁴	0	1	40	16

*As described in the Results, mutations previously attributed to *dab* are in fact *nrt* alleles.

[†]The percent of the expected progeny class of both pupae and viable adults of the indicated genotype is shown. A minimum of 400 animals was counted in each cross.

Number, X54999). The *nrt* allele on both the parental *Abl*[1] and the parental *Df(3L)st-j7* chromosome was found to be wild type. From the three chromosomes that failed to produce mAb BP106 reactivity [*Df(3L)st-j7, dab*[M2]; *Df(3L)st-j7,* dab[M29]; *Abl*[1]*, dab*[M54]] we found three independent null alleles of *nrt* (Fig. 4A). The *Df(3L)st-j7, dab*[M2] chromosome had a nonsense mutation, with the codon for L464 (TTG) being changed to an
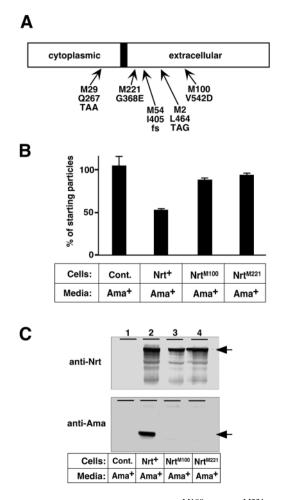
amber stop (TAG). The *Df(3L)st-j7, dab*[M29] chromosome also had a nonsense mutation, with the codon for Q267 (CAA) being changed to an ochre stop (TAA). The *Abl*[1]*, dab*[M54] chromosome was found to have an 11 bp deletion beginning in the codon for I405. The resulting frameshift would lead to the translation of two unique residues before a stop codon is reached. These mutations are all consistent with the mutagens used to generate the dominant enhancer mutations on these chromosomes, with the *M2* and *M29* alleles having been generated with EMS and the *M54* allele having been generated with X-rays (F. M. Hoffmann, personal communication).

As our molecular analysis of *dab* on the chromosomes that produced mAb BP106-reactivity (*Abl*[1]*, dab*[M100]*; Abl*[1]*, dab*[M221]) had failed to identify any telltale mutations, we also characterized the *nrt* alleles on these chromosomes. Interestingly, we found two independent missense mutations in *nrt* (Fig. 4A). The *Abl*[1]*, dab*[M100] chromosome carried a V542D missense mutation, and the *Abl*[1]*, dab*[M221] chromosome carried a G368E missense mutation. Both of these mutations map to the extracellular domain of Nrt, and both residues are conserved in the *A. gambiae* and *D. pseudoobscura* Nrt orthologs (data not shown). These mutations were consistent with the action of EMS that was used to generate the *M100* and *M221* mutations (F. M. Hoffmann, personal communication).

To explore these missense mutations further in *nrt*, we tested them in our S2 cell adhesion system. S2 cells expressing Nrt[+], Nrt[M100] (V542D) or Nrt[M221] (G368E) were exposed to wild-type Ama. As shown in Fig. 4C (lanes 2-4), all three Nrt proteins were expressed at comparable levels. However, although Nrt[+] expression mediated Ama[+] binding and cell aggregation (Fig. 4B,C, lane 2), Nrt[M100] and Nrt[M221] behaved similar to naïve S2 cells exposed to Ama[+]-containing supernatant. Neither mutant Nrt protein mediated Ama[+] binding (Fig. 4C, lanes 3, 4) and neither mutant Nrt protein mediated Ama-dependent cell:cell adhesion (Fig. 4B).

As different *nrt* null alleles had been created in different *Abl* mutant backgrounds, we were able to test the CNS phenotype of homozygous *Abl* mutant, *nrt* mutant embryos. As shown in Fig. 3F, embryos of the genotype *Df(3L)st-j7, nrt*[M2]*/Abl*[1]*, nrt*[M54] showed disruption of the axon architecture, with 63% of segments showing clear commissure defects (*n*=187). This phenotype is consistent with, but somewhat less severe than the phenotype generated by RNAi elimination of Abl and Nrt (Fig. 3C).

Taken together, our molecular characterization of both *dab* and *nrt* from these chromosomes carrying dominant enhancers of the *Abl* mutant phenotype strongly suggested the causative mutations in all cases were in *nrt* and not *dab*. No mutations in *dab* were found, while three independent null alleles of *nrt* and two independent missense alleles that eliminate Nrt function were identified. In light of these molecular data, we propose that these dominant enhancers of the *Abl* mutant phenotype, previously identified as *dab*[M2], *dab*[M29], *dab*[M54], *dab*[M100] and *dab*[M221] be renamed *nrt*[M2], *nrt*[M29], *nrt*[M54], *nrt*[M100] and *nrt*[M221].

DISCUSSION

Genetic screens for second-site modifiers are useful tools for identifying components of signaling networks (Hoffmann,

Fig. 4. Biochemical characterization of Nrt[M100] and Nrt[M221]. (A) The Nrt protein is represented. The N terminus is towards the left. The location of mutations *nrt*[M29], *nrt*[M221], *nrt*[M54], *nrt*[M2] and *nrt*[M100] are also shown. *nrt*[M54] is an 11 bp deletion that results in a frameshift (fs). (B) Graphical representation of the quantification of our S2 cell adhesion assay. Bars represent the percent of total particles at *t*=0 hours counted at *t*=8 hours. Values represent the average of two independent experiments; error bars show the standard error of the mean. (C) Immunoblots of S2 cell lysates from cell pull-down assays. (Top) Anti-Nrt immunoblots. Equivalent amounts of cell lysates were loaded in each lane. The arrow shows the migration of full-length Nrt. Lane 1: naïve S2 cells. Lane 2: S2 cells engineered to express Nrt[+]. Lane 3: S2 cells engineered to express Nrt[M100]. Lane 4: S2 cells engineered to express Nrt[M221]. Naïve S2 cells did not express Nrt, and all Nrt proteins were expressed from the pMET plasmid at comparable levels. (Bottom) Anti-Ama immunoblots. Equivalent amounts of cell lysates were loaded in each lane. The arrow shows the migration of full-length Ama. Lane 1: naïve S2 cells. Lane 2: Nrt[+]-expressing S2 cells. Lane 3: Nrt[M100]-expressing S2 cells. Lane 4: Nrt[M221]-expressing S2 cells. Only S2 cells expressing wild-type Nrt bound Ama.

1991; Thomas, 1993). Over the past decade, work in *Drosophila* has identified multiple modifiers of the *Abl* mutant phenotype. With the exception of the transcription factor *prospero* (Gertler et al., 1993), all of the dominant modifiers identified have been cytoplasmic and co-expressed with Abl in axons. The biochemical characterization of some of the proteins encoded by these dominant enhancers has lead to an emerging model whereby the Abl tyrosine kinase supplies multiple inputs into actin cytoskeleton dynamics in the growth cone (Lanier and Gertler, 2000).

In this study we report two novel dominant enhancers of the *Abl* mutant phenotype: *ama* and *nrt*. The dosage-sensitive genetic interactions between these genes and *Abl* provide unique information regarding Abl signaling networks. We have identified five independent *nrt* alleles that remove Nrt function. Three are null alleles (*nrt^M2*, *nrt^M29*, *nrt^M54*), while two (*nrt^M100* and *nrt^M221*) are missense alleles that behave as protein nulls (Fig. 4B,C). Thus, simply reducing wild-type Nrt activity in an *Abl*-null background impairs viability (Table 3), suggesting Abl and Nrt lie within one or more common signaling networks. The fact that these genetic combinations have clear effects on axon pathfinding (Fig. 3D,E), strongly suggests that at least one of these common signaling networks has its in vivo output in the growth cone. This is confirmed by the severe axon guidance phenotype produced by disruption of Abl and Nrt function through RNAi or homozygous zygotic mutation (Fig. 3C,F). Disruption of Abl and Nrt by zygotic mutation resulted in strong, but less severe CNS phenotypes than RNAi, probably as a result of elimination of maternally loaded Abl mRNA (Bennett and Hoffmann, 1992).

It had been shown previously that Ama and Nrt functionally interact to mediate cell:cell adhesion (Fremion et al., 2000). Heterozygous null alleles of *ama* have no detectable dominant effects on axon pathfinding in an *Abl*-mutant background (Fig. 1C,D), presumably because the biochemical activity of secreted Ama is not directly associated with the cytoplasmic tyrosine kinase activity of Abl. However, disruption of Abl and Ama by homozygous zygotic mutation (Fig. 1F) or by RNAi techniques (Table 2) did show clear synergistic disruptions of the CNS architecture. As with Abl and Nrt, the RNAi-induced phenotype was the more severe of the two, presumably because of the elimination of maternally supplied Abl mRNA.
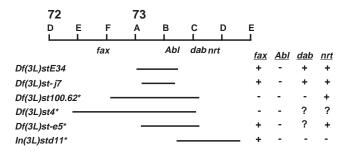
The identification of the unusual missense *ama* allele *ama^M109* as a strong dominant enhancer of the *Abl* mutant phenotype, affecting both viability and axon pathfinding (Table 1, Fig. 1B) strengthens our conclusion that Ama, Nrt and Abl are functionally intertwined in the growth cone. Ama^M109, which alters a cysteine residue needed to stabilize the first Ig domain of Ama (Fig. 2A), eliminates Ama homophilic adhesion but not the ability of Ama^M109 to bind Nrt (Fig. 2B-D), and this is probably responsible for its unique character. The biochemical activity of this protein is clearly not wild type, as its ability to support aggregation of Nrt-expressing S2 cells is impaired (Fig. 2B,C). Interestingly, Zhang and Filbin (Zhang and Filbin, 1998) have previously reported that destabilization of the Ig-domain of myelin-specific protein Po results in a dominant-negative effect. Po is a transmembrane protein with a single, extracellular Ig domain stabilized by a disulfide bond between C21 and C98. Chinese hamster ovary cells engineered

to express Po showed strong homophilic adhesion. Co-expression of a mutant Po, with an engineered C21A mutation, disrupted the aggregation mediated by wild-type Po.

Genetically, the *ama^M109* allele phenocopies heterozygosity for *nrt* in the *Abl^1/Abl^4* mutant background. Both genotypes result in 100% pre-pupal lethality (Table 1, Table 3), and both result in approximately one-third of embryo segments having defective commissures (Fig. 1B, Fig. 3D,E). Thus, it seems likely that, whatever its biochemical mode of action, the Ama^M109 protein disables Nrt activity in a way that simply reducing the dose of wild-type Ama (by heterozygous null mutation) does not.

To understand the function of Nrt in the CNS better, Speicher et al. (Speicher et al., 1998) carried out an extensive genetic analysis, looking for cell adhesion molecules (CAMs) that are functionally redundant to Nrt. This was achieved by generating animals null for *nrt* and null for a variety of other CAM-encoding genes in pair-wise combinations. Removal of Nrt does not result in a strong CNS phenotype (Table 2, Fig. 3B) (Speicher et al., 1998). Three different genetic combinations showed synergistic interactions in the CNS; *nrt* and *neuroglian* (*nrg*), *nrt* and *derailed* (*drl*), and *nrt* and *kekkon1* (*kek1*), with the *nrt, nrg* combination showing the most profound synergy (Speicher et al., 1998). This work suggests the role of Nrt in CNS cell adhesion is at least partially redundant to Nrg, Drl and Kek1. Interestingly, Elkins et al. (Elkins et al., 1990) report that *nrg* and *Abl* have no genetic interaction when the morphology of the CNS is assayed by mAb BP102 staining.

Whether Nrt-mediated adhesion provides novel inputs into Abl-mediated signaling networks in the growth cone or whether Nrt-mediated adhesion represents a novel output of the role of Abl in cytoskeleton dynamics can not be determined by the genetic experiments we have carried out. Intriguingly, Fremion et al. (Fremion et al., 2000) report that deletion of the cytoplasmic region of Nrt eliminates its ability to promote cell:cell adhesion. As many transmembrane cell adhesion molecules require functional interactions with the actin-based cytoskeleton (Petit and Thiery, 2000), it is plausible that Ama:Nrt-mediated adhesion requires interaction of the cytoplasmic region of Nrt with actin-based cytoskeleton components. We are currently conducting molecular genetic screens to identify protein:protein interactions involving the cytoplasmic domain of Nrt to clarify this issue.

Our molecular and genetic characterization of *nrt* as a dominant enhancer of the *Abl* mutant phenotype has shown that all five mutations previously attributed to *dab* are *nrt* alleles (Fig. 4A). How were these mutations initially attributed to *dab*? Originally it was observed that deletions that remove *Abl* as well as genes both proximal and distal to *Abl* (*Df(3L)st100.62*, *Df(3L)st4*, *Df(3L)st-e5*) or only genes proximal to *Abl* (*In(3L)std11*), showed a dominant enhancement of the *Abl* mutant phenotype (Fig. 5) (Henkemeyer et al., 1987). The EMS-induced mutations *M2* and *M29* mapped tightly to *Df(3L)st-j7* and failed to complement *In(3L)std11*, leading to the hypothesis that these were alleles of a dominant enhancer gene lying proximal to *Abl* (Gertler et al., 1989). The key observation that lead to *dab* seems to have been that *Df(3L)stE34* did not exhibit dominant enhancement of the *Abl* mutant phenotype, while *Df(3L)st100.62* did show dominant enhancement of the *Abl* mutant phenotype (Fig. 5) (Gertler

	fax	Abl	dab	nrt
Df(3L)stE34	+	-	+	+
Df(3L)st-j7	+	-	+	+
Df(3L)st100.62*	-	-	-	+
Df(3L)st4*	-	-	?	?
Df(3L)st-e5*	+	-	?	+
In(3L)std11*	+	-	-	-

Fig. 5. Cytological region 72D; 73E. The cytological map is represented across the top; the centromere is towards the right. The placements of the *fax*, *Abl*, *dab* and *nrt* genes are shown. Solid lines represent the cytological extent of the chromosomal deficiencies as reported in FlyBase (http://flybase.bio.indiana.edu). The genotype of these deficiencies with regard to *fax*, *Abl*, *dab* and *nrt* is indicated to the right. Based on data reported previously (Henkemeyer et al., 1987), deficiencies that dominantly enhance the *Abl* mutant phenotype are indicated by asterisks. Although the distal breakpoint of *Df(3L)st100.62* is listed as 72F3-4 in FlyBase and *fax* is placed in 72E5-F1, Hill et al. (Hill et al., 1995) report that *Df(3L)st100.62* is null for *fax*. *In(3L)std11* contains the deficiency shown as well as an inversion (73E1-2).

et al., 1989). Molecular characterization of the proximal breakpoints of these deletions showed *Df(3L)st100.62* removed the *dab* gene, while *Df(3L)stE34* left *dab* intact (Gertler et al., 1993), suggesting that *dab* was the gene proximal to *Abl* responsible for the dominant enhancement of the *Abl* mutant phenotype. However, in retrospect, the difference in genetic activity between *Df(3L)st100.62* and *Df(3L)stE34* can be accounted for by the difference in the distal breakpoints of these chromosomes. Null mutations in *fax* dominantly enhance the *Abl* mutant phenotype (Hill et al., 1995). On its distal end *Df(3L)st100.62* removes *fax* (Hill et al., 1995) while *Df(3L)stE34* leaves *fax* intact (Fig. 5). Thus, although *nrt^{M2}* and *nrt^{M29}* do lie proximal to *Abl*, *Df(3L)st100.62* has been shown to be wild type for *nrt* (de la Escalera et al., 1990) and therefore the proximal breakpoint of *Df(3L)st100.62* does not uncover the dominant enhancer gene identified by the *M2* and *M29* mutations.

It has also been reported that multiple copies of a P-element cosmid vector that contains 35 kb of genomic DNA containing the *dab* transcription unit could partially rescue the pre-pupal lethality associated with the *M2* allele in the *Abl* mutant background (Gertler et al., 1993). To our knowledge, this P-element is no longer available. Molecular mapping showed this cosmid extended only ~10 kb proximal to *dab*, and no embryonic transcripts proximal to *dab* were identified by this cosmid through northern blotting or when it was used to screen a cDNA library (Gertler et al., 1993). Thus, it seems unlikely that this cosmid vector could have included the *nrt* gene. The rescue provided by this cosmid was interpreted as confirming the identification of *M2* as a *dab* allele. However, in light of our molecular evidence, we believe these data indicate that expression, or perhaps overexpression, of *dab* can, by some unknown mechanism, partially rescue the lethality caused by heterozygosity at *nrt* in the *Abl*-mutant background. This potential interplay between *nrt* and *dab* in *Drosophila* is intriguing, and merits further exploration. However, our

sequence data confirms the *M2*, *M29*, *M54*, *M100* and *M221* mutations are *nrt* alleles. These findings will necessitate a re-evaluation of other studies that have reported genetic interactions with these alleles (Giniger, 1998; Hill et al., 1995; Le and Simion, 1998).

Our re-examination of the work of others in light of the fact that these alleles are *nrt* mutations has revealed a startling fact: there may be yet another dominant enhancer of the *Abl* mutant phenotype in the 73A-C region. As with *Df(3L)st100.62*, the dominant enhancement of the *Abl* mutant phenotype reported for *Df(3L)st4* (Henkemeyer et al., 1987) is likely to be due to its removal of the *fax* gene, distal to *Abl* (Fig. 5). However, Henkemeyer et al. (Henkemeyer et al., 1987) have also shown that *Df(3L)st-e5* is a strong dominant enhancer of the *Abl* mutant phenotype. Based on its reported cytology, *Df(3L)st-e5* is wild-type for *fax* (Fig. 5). The work of de la Escalera et al. (de la Escalera et al., 1990) has shown the *Df(3L)st-e5* chromosome is wild type for *nrt*. Thus, this deficiency apparently uncovers another gene in the 73A-C region that can dominantly enhance the *Abl* mutant phenotype. We are currently pursuing the identity of this gene.

This report is not the first description of genetic interactions between *Abl* and genes encoding cell adhesion molecules. Similar to the strong phenotypic effects on CNS architecture that we have described in animals homozygous mutant for *Abl* and *nrt* (Fig. 3C,F), Elkins et al. (Elkins et al., 1990) have found that animals homozygous mutant for both *Abl* and *fasciclinI* (*fasI*) show a mutant phenotype affecting midline crossing of commissural axons. Unlike the present study, however, heterozygous mutations in *fasI* had no effect on the *Abl* mutant phenotype. The discovery of dosage-sensitive genetic interactions, such as that between *Abl* and *nrt*, may indicate that the proteins encoded by these two genes are biochemically linked. The continued search for dosage-sensitive modifiers of the *Abl* mutant phenotype, and the continued biochemical characterization of these modifiers will undoubtedly deepen our picture of the molecular machinery guiding neuronal growth cones.

REFERENCES

Awasaki, T., Saitoh, M., Sone, M., Suzuki, E., Sakai, R., Ito, K. and Hama, C. (2000). The Drosophila Trio plays an essential role in patterning of axons by regulating their directional extension. *Neuron* **26**, 119-131.

Barthalay, Y., Hipeau-Jacquotte, R., de la Escalera, S., Jimenez, F. and Piovant, M. (1990). Drosophila neurotactin mediates heterophilic cell adhesion. *EMBO J.* **9**, 3603-3609.

Bashaw, G. J., Kidd, T., Murray, D., Pawson, T. and Goodman, C. S. (2000). Repulsive axon guidance: Abelson and Enabled play opposing roles downstream of the Roundabout receptor. *Cell* **101**, 703-715.

Bateman, J., Shu, H. and van Vactor, D. (2000). The guanine nucleotide exchange factor Trio mediates axonal development in the Drosophila embryo. *Neuron* **26**, 93-106.

Bear, J. E., Loureiro, J. J., Fassler, R., Wehland, J. and Gertler, F. B.

(2000). Negative regulation of fibroblast motility by Ena/VASP proteins. *Cell* **101**, 717-728.

Bear, J. E., Svitkina, T. M., Krause, M., Schafer, D. A., Loureiro, J. J., Strasser, G. A., Maly, I. V., Chaga, O. Y., Cooper, J. A., Borisy, G. G. et al. (2002). Antagonism between Ena/VASP proteins and actin filament capping regulates fibroblast motility. *Cell* **109**, 509-521.

Belote, J. M., Hoffmann, F. M., McKeown, M., Chorsky, R. L. and Baker, B. S. (1990). Cytogenetic analysis of chromosome region 73AD of Drosophila melanogaster. *Genetics* **125**, 783-793.

Bennett, R. L. and Hoffmann, F. M. (1992). Increased levels of the Drosophila Abelson tyrosine kinase in nerves and muscles: subcellular localization and mutant phenotypes imply a role in cell-cell interactions. *Development* **116**, 953-966.

Bunch, T. A., Grinblat, Y. and Goldstein, L. S. (1988). Characterization and use of the Drosophila metallothionein promoter in cultured Drosophila melanogaster cells. *Nucl. Acids Res.* **16**, 1043-1061.

Cooley, L., Verheyen, E. and Ayers, K. (1992). *chickadee* encodes a profilin required for intercellular cytoplasm transport during Drosophila oogenesis. *Cell* **69**, 173-184.

Diederich, R. J., Merrill, V. K., Pultz, M. A. and Kaufman, T. C. (1989). Isolation, structure, and expression of labial, a homeotic gene of the Antennapedia Complex involved in Drosophila head development. *Genes Dev.* **3**, 399-414.

de la Escalera, S., Bockamp, E. O., Moya, F., Piovant, M. and Jimenez, F. (1990). Characterization and gene cloning of Neurotactin, a Drosophila transmembrane protein related to cholinesterases. *EMBO J.* **9**, 3593-3601.

Elkins, T., Zinn, K., McAllister, L., Hoffmann, F. M. and Goodman, C. S. (1990). Genetic analysis of a Drosophila neural cell adhesion molecule: interaction of Fasciclin I and Abelson tyrosine kinase mutations. *Cell* **60**, 565-575.

Fremion, F., Darboux, I., Diano, M., Hipeau-Jacquotte, R., Seeger, M. A. and Piovant, M. (2000). Amalgam is a ligand for the transmembrane receptor Neurotactin and is required for Neurotactin mediated cell adhesion and axon fasciculation in Drosophila. *EMBO J.* **19**, 4463-4472.

Gallagher, E., Howell, B. W. and Hawkes, R. (1998). Cerebellar abnormalities in the disabled (mdab-1) mouse. *J. Comp. Neurol.* **402**, 238-251.

Gertler, F. B., Bennett, R. L., Clark, M. J. and Hoffmann, F. M. (1989). Drosophila abl tyrosine kinase in embryonic CNS axons: a role in axonogenesis is revealed through dosage-sensitive interactions with disabled. *Cell* **58**, 103-113.

Gertler, F. B., Doctor, J. S. and Hoffmann, F. M. (1990). Genetic suppression of mutations in the Drosophila abl proto-oncogene homolog. *Science* **248**, 857-860.

Gertler, F. B., Hill, K. K., Clark, M. J. and Hoffmann, F. M. (1993). Dosage-sensitive modifiers of Drosophila abl tyrosine kinase function: Prospero, a regulator of axonal outgrowth, and disabled, a novel tyrosine kinase substrate. *Genes Dev.* **7**, 441-453.

Gertler, F. B., Comer, A. R., Juang, J.-L., Ahern, S. M., Clark, M. J., Liebl, E. C. and Hoffmann, F. M. (1995). enabled, a dosage-sensitive suppressor of mutations in the Drosophila Abl tyrosine kinase, encodes an Abl substrate with SH3 domain-binding properties. *Genes Dev.* **9**, 521-533.

Gertler, F. B., Niebuhr, K., Reinhard, M., Wehland, J. and Soriano, P. (1996). Mena, a relative of VASP and Drosophila enabled, is implicated in the control of microfilament dynamics. *Cell* **87**, 1-20.

Giniger, E. (1998). A role for Abl in Notch signaling. *Neuron* **20**, 667-681.

Goh, K. L., Cai, L., Cepko, C. L. and Gertler, F. B. (2002). Ena/VASP proteins regulate cortical neuronal positioning. *Curr. Biol.* **12**, 565-569.

Henkemeyer, M. J., Gertler, F. B., Goodman, W. and Hoffmann, F. M. (1987). The Drosophila Abelson proto-oncogene homolog: Identification of mutant alleles that have pleiotropic effects late in development. *Cell* **51**, 821-828.

Hill, K. K., Bedian, V., Juang, J.-L. and Hoffmann, F. M. (1995). Genetic interactions between Drosophila Abelson (Abl) tyrosine kinase and failed axon connections (fax), a novel protein in axon bundles. *Genetics* **141**, 595-606.

Hoffmann, F. M. (1991). Drosophila abl and genetic redundancy in signal transduction. *Trends Genet.* **7**, 351-355.

Hortsch, M., Patel, N. H., Bieber, A. J., Traquina, Z. R. and Goodman, C. S. (1990). *Drosophila* neurotactin, a surface glycoprotein with homology to serine esterases, is dynamically expressed during embryogenesis. *Development* **110**, 1327-1340.

Howell, B. W., Gertler, F. B. and Cooper, J. A. (1997). Mouse disabled (mDab): a src binding protein implicated in neuronal development. *EMBO J.* **16**, 121-132.

Kennerdell, J. R. and Carthew, R. W. (1998). Use of dsRNA-mediated genetic interference to demonstrate that frizzled and frizzled2 act in the wingless pathway. *Cell* **95**, 1017-1026.

Kidd, T., Bland, K. S. and Goodman, C. S. (1999). Slit is the midline repellent for the Robo receptor in Drosophila. *Cell* **96**, 785-794.

Lanier, L. M. and Gertler, F. B. (2000). From Abl to actin: the role of the Abl tyrosine kinase and its associated proteins in growth cone motility. *Curr. Opin. Neurobiol.* **10**, 80-87.

Lanier, L. M., Gates, M. A., Witke, W., Menzies, A. S., Kwiatkowski, D., Soriano, P. and Gertler, F. B. (1999). Mena is required for neurulation and commissure formation. *Neuron* **22**, 313-325.

Le, N. and Simion, M. A. (1998). Disabled is a putative adaptor protein that functions during signaling by the sevenless receptor tyrosine kinase. *Mol. Cell. Biol.* **18**, 4844-4854.

Liebl, E. C., Forsthoefel, D. J., Franco, L. S., Sample, S. H., Hess, J. E., Cowger, J. A., Chandler, M. P., Shupert, A. M. and Seeger, M. A. (2000). Dosage-sensitive, reciprocal genetic interactions between the Abl tyrosine kinase and the putative GEF trio reveal trio's role in axon pathfinding. *Neuron* **26**, 107-118.

Newsome, T. P., Schmidt, S., Dietzl, G., Keleman, K., Åsling, B., Debant, A. and Dickson, B. J. (2000). Trio combines with Dock to regulate Pak activity during photoreceptor axon guidance in Drosophila. *Cell* **101**, 283-294.

Patel, N. H., Snow, P. M. and Goodman, C. S. (1987). Characterization and cloning of fasciclin III: a glycoprotein expressed in Drosophila. *Cell* **48**, 975-988.

Petit, V. and Thiery, J.-P. (2000). Focal adhesions: structure and dynamics. *Biol. Cell* **92**, 477-494.

Renfranz, P. J. and Beckerle, M. C. (2002). Doing (F/L)PPPPs: EVH1 domains and their proline-rich partners in cell polarity and migration. *Curr. Opin. Cell Biol.* **14**, 88-103.

Rhee, J., Mahfooz, N. S., Arregui, C., Lilien, J., Balsmo, J. and van Berkum, M. F. A. (2002). Activation of the repulsive receptor Roundabout inhibits N-cadherin-mediated cell adhesion. *Nat. Cell Biol.* **4**, 798-805.

Seeger, M., Tear, G., Ferres-Marco, D. and Goodman, C. S. (1993). Mutations affecting growth cone guidance in Drosophila: genes necessary for guidance toward or away from the midline. *Neuron* **10**, 409-426.

Seeger, M. A., Haffley, L. and Kaufman, T. C. (1988). Characterization of amalgam: a member of the immunoglobulin superfamily from Drosophila. *Cell* **55**, 589-600.

Speicher, S., Garcia-Alonso, L., Carmena, A., Martin-Bermudo, M. D., de la Escalera, S. and Jimenez, F. (1998). Neurotactin functions in concert with other identified CAMs in growth cone guidance in Drosophila. *Neuron* **20**, 221-233.

Thomas, J. H. (1993). Thinking about genetic redundancy. *Trends Genet.* **19**, 395-398.

Van Etten, R. A. (1999). Cycling, stressed-out and nervous: cellular functions of c-Abl. *Trends Cell Biol.* **9**, 179-186.

Ware, M. L., Fox, J. W. and Walsh, C. A. (1997). Aberrant splicing of a mouse disabled homolog, mdab1, in the scrambler mouse. *Neuron* **19**, 239-249.

Wills, Z., Marr, L., Zinn, K., Goodman, C. S. and van Vactor, D. (1999). Profilin and the Abl tyrosine kinase are required for motor axon outgrowth in the Drosophila embryo. *Neuron* **22**, 291-299.

Willis, Z., Emerson, M., Rusch, J., Bikoff, J., Baum, B., Perrimon, N. and van Vactor, D. (2002). A Drosophila homolog of cyclase-associated proteins collaborates with the Abl tyrosine kinase to control midline axon pathfinding. *Neuron* **36**, 611-622.

Zhang, K. and Filbin, M. T. (1998). Myelin Po protein mutated at Cys21 has a dominant-negative effect on adhesion of wild type Po. *J. Neurosci. Res.* **53**, 1-6.